JOURNAL OF AIRCRAFT
Vol. 32, No. 5, September–October 1995

Pitch Rate and Pitch-Axis Location Effects on Vortex Breakdown Onset

Miguel R. Visbal* and Raymond E. Gordnier*
U.S. Air Force Wright Laboratory, Wright–Patterson Air Force Base, Ohio 45433-7913

Computational results are presented for the onset of vortex breakdown above a 75-deg sweep delta wing subject to a ramp-type pitch maneuver to high angle of attack. The flows are simulated by solving the full three-dimensional unsteady Navier–Stokes equations on a moving grid using the implicit Beam–Warming algorithm. An assessment of the effects of numerical resolution, and comparison with experiment are employed to validate the computational approach. The effects of pitch rate and pitch-axis location are examined. For a range of these parameters, it is found that either increasing pitch rate or moving the axis downstream results in a larger angular delay of vortex bursting. These effects are correlated with the motion-induced effective incidence along the wing. For fixed pitch rate, the change in pivot location is equivalent to a shift in time without significant alteration of the flow structure.

Nomenclature

C	=	wing chord
C_p	=	pressure coefficient, $2(p - p_\infty)/\rho U_\infty^2$
M_∞	=	freestream Mach number
t	=	time
t^+	=	nondimensional time, tU_∞/C
U, V, W	=	velocity components in wing frame of reference
U_∞	=	freestream velocity
u, v, w	=	velocity components in inertial frame of reference
X, Y, Z	=	coordinate system attached to the wing
X_b	=	chordwise location of vortex breakdown
X_0	=	pitch axis location
x, y, z	=	inertial frame of reference
α	=	geometric angle of attack
ξ, η, ζ	=	transformed coordinates
Ω	=	pitch rate, rad/s
Ω_0^+	=	nondimensional pitch rate, $\Omega_0 C/U_\infty$

Introduction

STUDY of the unsteady aerodynamics of maneuvering delta wings is motivated by continued interest in the expansion of the operational envelope of current and future combat aircraft.[1] In recent years, both experimental[2–5] and computational[6–8] studies of pitching delta wings have been conducted in an effort to elucidate the complex fluid physics encountered in the high-angle-of-attack regime. The reviews by Ashley et al.[9] and Rockwell[10] may be consulted for an extensive compilation of related work.

Experiments show that at high incidence, the vortical flowfield about a delta wing may exhibit a variety of challenging fluid dynamic phenomena not yet fully understood. These include vortex breakdown, flow asymmetry, vortex/shock interactions, three-dimensional separation, and stall. For the case of rapid maneuvering, interrelated effects due to type and rate of wing motion, pitch-axis location, and range of angle of attack must be considered, in addition to the effects of compressibility and wing geometry, already present in the static situation.

Of particular interest in the present investigation is the onset of vortex breakdown above a delta wing performing a ramp-type pitch maneuver from an initial moderate incidence, for which breakdown is absent, to a high angle of attack at which breakdown would have occurred in the static case. This article focuses on the specific effects of pitch rate and pivot location on the initiation and propagation of vortex bursting above the wing.

The effects of pitch rate have been previously investigated experimentally,[2–5] with emphasis on the lag of vortex breakdown and on the overshoot in the wing aerodynamic loads as compared to the static situation. In order to explain the observed lag in the onset of bursting, further quantitative information is required on the vortex core development at various instants during the pitch motion. This can help elucidate, for instance, the role of the axial pressure gradient imposed on the vortex by the wing motion.

The effect of pitch-axis location has not been investigated previously for a delta wing in a ramp-type maneuver. This effect was considered in Ref. 11, however, for a delta wing undergoing sinusoidal oscillations. Pivot location is of importance when correlating experiments performed with different pitch-axis locations ranging from the wing apex[12] to the trailing edge.[13] In addition, this parameter would be expected to be important when considering canard/wing configurations or double-delta wings maneuvering at sufficiently high pitch rates.

The main objective of the present computations is to investigate the effects of pitch rate and pitch-axis location on the onset of vortex breakdown above a delta wing pitching to high angle of attack. To achieve this objective, calculations are performed for a 75-deg sweep flat-plate delta wing that is pitched at a constant rate from an initial angle of attack of 25 deg to a final angle of 50 deg. Two different pitch rates and pitch axis locations are employed in order to study the effects of these parameters on the breakdown onset for laminar conditions. The flows are simulated by solving the unsteady three-dimensional compressible Navier–Stokes equations on a moving grid using a time-accurate implicit solver. An assessment of numerical resolution adequacy, as well as comparison with experiment are performed in order to validate the computational approach.

Presented as Paper 94-0538 at the AIAA 32nd Aerospace Sciences Meeting and Exhibit, Reno, NV, Jan. 10–13, 1994; received Feb. 4, 1994; revision received Oct. 12, 1994; accepted for publication Oct. 24, 1994.

*Aerospace Engineer, CFD Research Branch, Aeromechanics Division. Senior Member AIAA.

Methodology

Governing Equations and Numerical Procedure

The governing equations are the full unsteady, three-dimensional compressible Navier–Stokes equations written in strong conservation law form.[14] Closure of this system of equations is provided by the perfect gas law, Sutherland's viscosity formula and the assumption of a constant Prandtl number ($Pr = 0.72$). In order to deal with the case of external flow past a body in general motion, a time-dependent coordinate transformation is incorporated.

The governing equations are numerically solved employing the implicit approximate-factorization Beam–Warming algorithm.[15] The scheme is formulated using Euler implicit time-differencing and second-order finite difference approximations for all spatial derivatives. Fourth-order nonlinear dissipation is added to control spurious numerical oscillations.[16] Newton subiterations[17,18] are also incorporated in order to reduce linearization and factorization errors, thereby improving the temporal accuracy and stability properties of the algorithm. A fully vectorized, time-accurate, three-dimensional Navier–Stokes solver has been developed using this scheme. The code has been validated for a variety of both steady and unsteady flowfields.[7,18–22]

Grid Structure and Boundary Conditions

The computational grid topology for the flat-plate delta wing is of the H-H type[18] and is obtained using simple algebraic techniques. Following the numerical resolution study of Refs. 7 and 23, a grid with 141 × 115 × 118 points in the ξ, η, and ζ directions, respectively, was selected for the laminar computations. The ξ, η, and ζ directions correspond to the streamwise, spanwise, and normal directions relative to the delta wing (see Fig. 1). The minimum spacing normal to the wing is $\Delta Z/C = 0.0001$, the spacing along the wing leading edge varies from $\Delta Y/C = 5 \times 10^{-5}$ at the apex to $\Delta Y/C = 5 \times 10^{-4}$ at the trailing edge, and the streamwise spacing on the wing is $\Delta X/C = 0.01$. The far-field boundaries are located two chord lengths away from the delta wing. The effect of far-field boundary placement was investigated[20] for an 80-deg sweep delta wing at 30-deg angle of attack, and found to be insignificant when the distance from the far-field boundary to the wing was increased from 1.5 to 3.0 chord lengths.

The boundary conditions are implemented as described in Ref. 18. On the lower, upper, lateral, and upstream boundaries, characteristic conditions are specified. On the downstream boundary, flow variables are extrapolated from the interior. Symmetry conditions are imposed along the midplane of the wing. On the wing surface, the following conditions are applied:

$$\boldsymbol{u} = \boldsymbol{u}_b$$

$$T = T_a$$

$$\frac{\partial p}{\partial \zeta} = -\rho \boldsymbol{a}_b \cdot \hat{n}$$

where $\hat{n}$ denotes the surface normal, T_a is the adiabatic wall temperature, and $\boldsymbol{u}_b$ and $\boldsymbol{a}_b$ are the velocity and acceleration at the surface of the pitching wing given by (see Fig. 1)

$$\boldsymbol{u}_b = \boldsymbol{\Omega} \times (\boldsymbol{r}_b - \boldsymbol{r}_0)$$

$$\boldsymbol{a}_b = \frac{d\boldsymbol{\Omega}}{dt} \times (\boldsymbol{r}_b - \boldsymbol{r}_0) + \boldsymbol{\Omega} \times [\boldsymbol{\Omega} \times (\boldsymbol{r}_b - \boldsymbol{r}_0)]$$

in terms of the instantaneous pitch rate $\boldsymbol{\Omega} = \Omega_f$ and the pitch axis location $\boldsymbol{r}_0$. In the present study, a ramp-type, pitch-and-hold maneuver is considered in which the wing pitch rate accelerates from zero to a constant value Ω_0, and then decelerates as it reaches its final incidence. In order to avoid an infinite angular acceleration, a smooth variation of the pitch rate is prescribed at the beginning and end of the maneuver. During the acceleration phase, the pitch rate $\Omega(t^+)$ varies as follows:

$$\Omega(t^+) = \Omega_0[3(t^+/t_0^+)^2 - 2(t^+/t_0^+)^3], \qquad 0 \le t^+ \le t_0^+ \tag{1a}$$

where t_0^+ denotes the nondimensional time required by the wing to attain its final constant pitch rate Ω_0. A similar variation is employed during deceleration. Namely,

$$\Omega(t^+) = \Omega_0 \left[1 - 3 \left(\frac{t_f^+ - t_0^+ - t^+}{t_0^+} \right)^2 - 2 \left(\frac{t_f^+ - t_0^+ - t^+}{t_0^+} \right)^3 \right] \tag{1b}$$

$$t_f^+ - t_0^+ \le t^+ \le t_f^+$$

where $t_f^+ = t_0^+ + (\alpha_f - \alpha_i)/\Omega_0^+$ denotes the time at which the wing comes to a full stop, and α_i and α_f are the initial and final angle of attack, respectively. An example of the temporal variation of α and Ω is shown in Fig. 2.

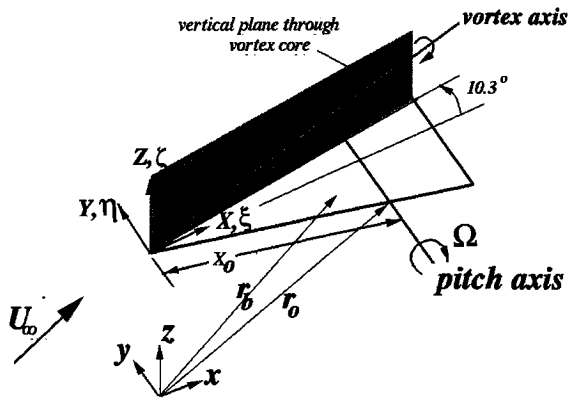

Fig. 1 Pitching delta wing configuration.

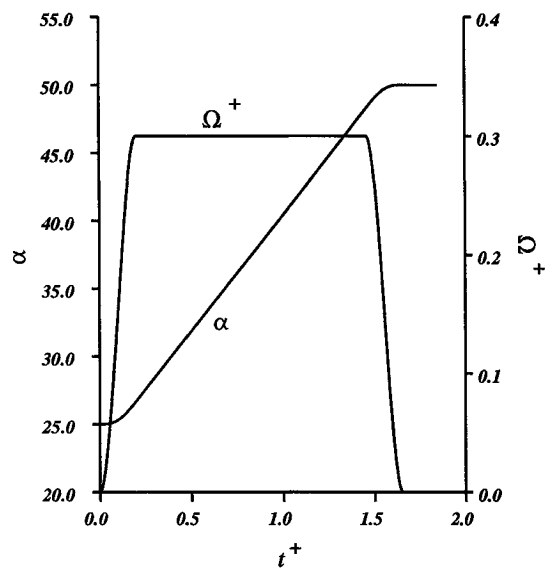

Fig. 2 Variation of angle of attack and angular velocity for $\Omega_0^+ = 0.3$ and $t_0^+ = 0.2$.

Results

All calculations are performed for a 75-deg sweep flat-plate delta wing. The angle of attack varies from $\alpha_i = 25$ deg to a

final angle $\alpha_f = 50$ deg. Two different values for the nondimensional pitch rate are considered ($\Omega_0^+ C/U_\infty = 0.1, 0.3$). The parameter i_0^+ in Eqs. (1a) and (1b) is set equal to 0.1 and 0.2 for the lower and higher pitch rate, respectively. Two pitch-axis locations ($X_0/C = 0.0, 1.0$) are investigated, which correspond to the apex and trailing edge of the wing. Laminar computations are performed for a chord Reynolds number $Re_C = 9.2 \times 10^3$ and a freestream Mach number $M_\infty = 0.2$. These conditions are selected to facilitate comparison with the experiments of Magness et al.[13] and Lin and Rockwell.[24]

Validation of Computed Results

Before addressing the parametric effects on the onset of vortex breakdown, the solution procedure is validated by a numerical resolution study and by comparison with available experimental data.

The sensitivity of the computed flowfield to numerical resolution was investigated for $\Omega_0^+ = 0.3$ and $X_0/C = 1.0$ and is described in detail in Refs. 7 and 23. For the grids and time-step sizes considered, the effects of spatial and temporal resolution on the lift, drag, and pitching moment coefficient histories were found[7] to be insignificant during the onset and initial stages of breakdown. The influence of grid resolution and time-step size on the instantaneous vortex burst location (as determined from the stagnation point in the vortex core) is reproduced here, for convenience, in Fig. 3. Despite the variations of time step (Δt^+) and streamwise grid spacing on the wing by a factor of 2 and 4, respectively, all computations agree reasonably well with each other for $t^+ \leq 2.5$. Further comparison of the flow structure computed using the different grids can be found in Refs. 7 and 23. The computed instantaneous position of vortex breakdown for this case is also in good agreement with the experimental results of Lin and Rockwell,[24] shown in Fig. 3. Comparison of the computed and experimental flow structure in the breakdown region is provided in Ref. 7, on a vertical plane through the center of the vortex. Both experiment and computation showed the formation of a bubble-type breakdown with maximum reversed velocity magnitudes within the bubble of the order of the freestream value.

The effect of grid resolution on the computed instantaneous vortex breakdown location for two other cases is shown in Fig. 4. Here again, the onset and propagation speed of bursting displays little sensitivity to the change in grid spacing.

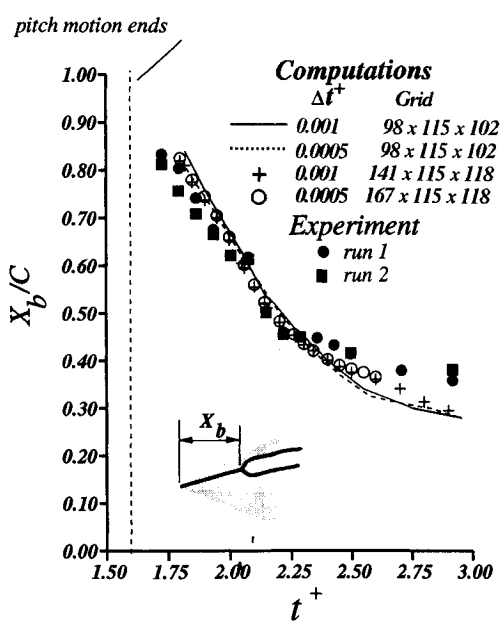

Fig. 3 Computed and experimental[24] instantaneous breakdown location for $\Omega_0^+ = 0.3$ and $X_0/C = 1.0$.

From the experimental work of Ref. 13, the crossflow topology at $X/C = 0.79$ and $\alpha = 45$ deg is available for $\Omega_0^+ = 0.1$ and $X_0/C = 1.0$. A comparison of the computed and experimental crossflow topologies, provided in Fig. 5, shows qualitative agreement, with the exception of asymmetric effects not reproducible in the symmetric calculation. In both computation and experiment, the crossflow pattern of the primary vortex is characterized by a repelling focus and by the lack of entrainment into the core of the sectional streamline emanating from the wing leading edge. The presence of the repelling focus is associated with axial compression along

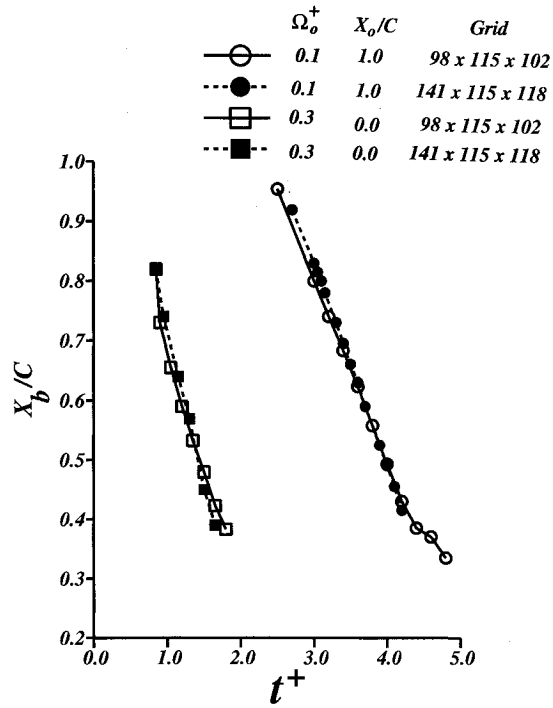

Fig. 4 Effect of grid resolution on computed breakdown location.

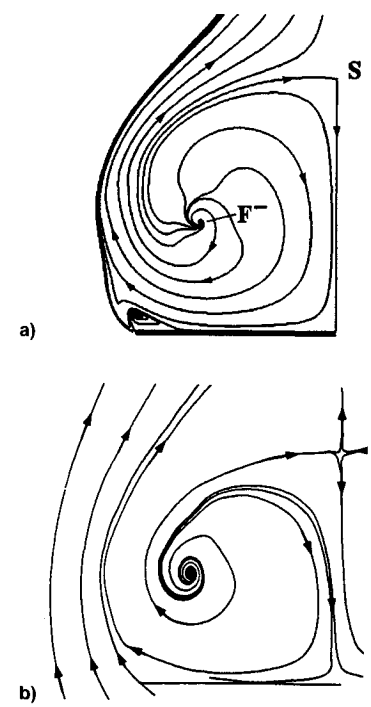

Fig. 5 Comparison of computed and experimental crossflow topologies at $X/C = 0.79$ and $\alpha = 45$ deg ($\Omega_0^+ = 0.1$, $X_0/C = 1.0$): a) computation and b) experiment.[13]

the vortex core.[13,25] At the instant corresponding to Fig. 5, the breakdown point is located just upstream of the chordwise station shown.

The above assessment of numerical resolution effects and the favorable comparison with the experimental measurements indicate that, at low Reynolds numbers, the computational approach adequately captures the onset of vortex breakdown above a pitching delta wing.

Effects of Pitch Rate and Pitch-Axis Location

In this section, the effects of pitch rate and pivot axis location are discussed with emphasis on how these parameters influence the onset and initial propagation of vortex breakdown above the wing.

Figures 6a and 6b show the computed instantaneous position of vortex breakdown for all cases in terms of nondimensional time and angle of attack, respectively. The experimentally determined[13] breakdown location for static conditions is also included in Fig. 6b, for reference purposes. Based on Fig. 6, several observations can be made. Increasing the pitch rate results in an angular delay of the onset of breakdown relative to the static situation. This predicted lag is consistent with the previously cited experimental observations. This effect is more pronounced when the axis is located at the trailing edge. In particular, for $\Omega_0^+ = 0.3$ and $X_0/C = 1.0$, vortex bursting only occurs over the wing after the completion of the pitching motion at $\alpha = 50$ deg, in agreement with the experiment (see Fig. 3). It can also be seen in Fig. 6a that the initial speed of propagation of the breakdown point, $d(X_b/C)/dt^+$, increases with Ω_0^+.

For fixed Ω_0^+, placing the axis further downstream also causes a delay in vortex breakdown onset. This delay is larger at the higher pitch rate. It can also be noted in Fig. 6a that for $\Omega_0^+ = 0.1$ moving the pitch axis from the apex to the trailing edge does not significantly affect the initial breakdown propagation speed.

A complete explanation is not currently available for the observed lag in the onset of vortex breakdown above a rapidly pitching wing. However, several aspects are discussed that provide some insight into the pitch rate and pitch axis trends noted above. The onset of breakdown is controlled in part by time-lag mechanisms in the vortex core development, as well as by the potential flow effects due to the wing motion that produces a change of effective angle of attack and a motion-induced longitudinal camber.[26] These features are interrelated, since lags along the vortex core are expected to depend on the axial core velocity, which is itself affected by the wing pitching motion.

The instantaneous effect of pitch rate and axis location on the effective local angle of attack is described briefly, in reference to the sketch of Fig. 7a. For a given pitch rate and

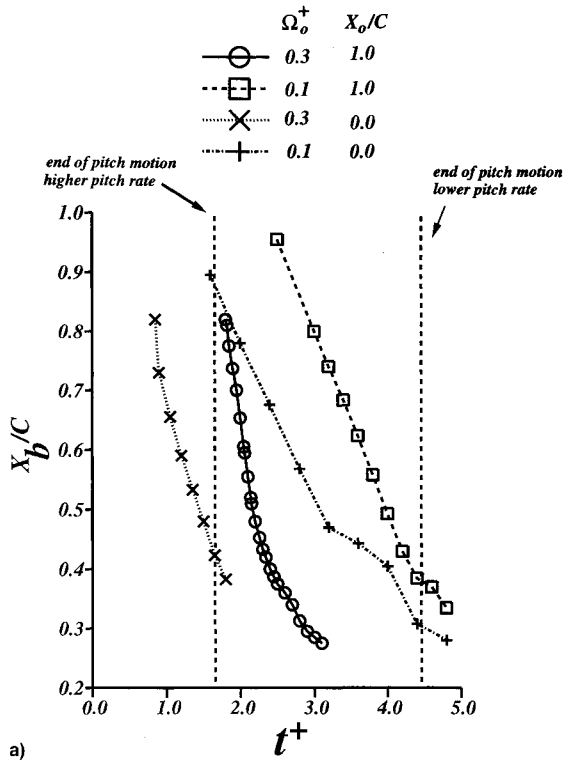

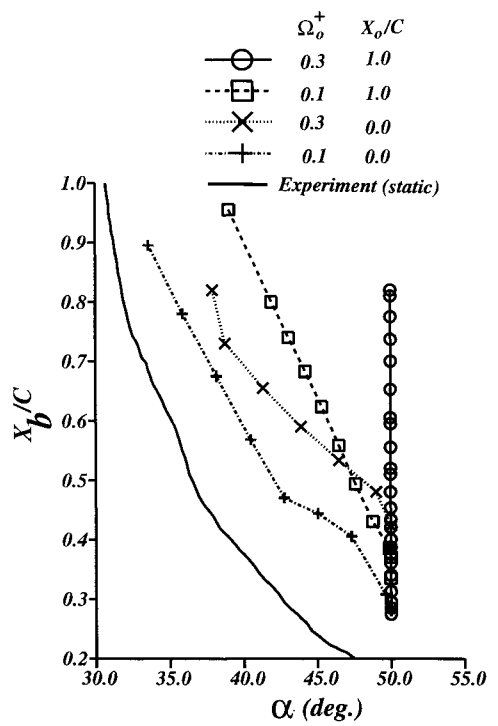

Fig. 6 Effect of Ω_0^+ and X_0/C on vortex breakdown location.

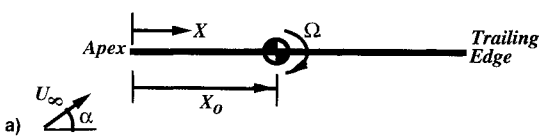

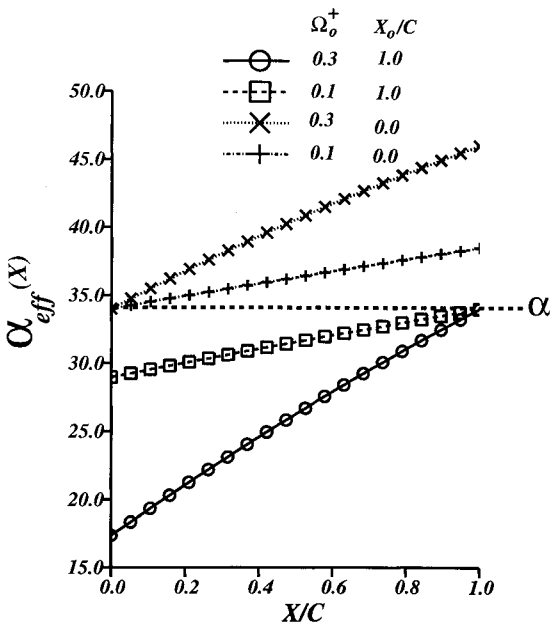

Fig. 7 Motion-induced effective angle of attack.

pivot location, the motion-induced effective angle of attack at a given chordwise station, $\alpha_{\text{eff}}(X)$, can be shown to be

$$\alpha_{\text{eff}}(X) = \tan^{-1}\left[\tan\alpha - \frac{\Omega^+(X_0/C - X/C)}{\cos\alpha}\right]$$

Figure 7b shows the variation of α_{eff} for the cases considered at a geometric angle of attack $\alpha = 34$ deg. It can be seen that for all cases, the pitch motion induces an apparent positive longitudinal camber (i.e., the local incidence increases from the apex to the trailing edge). In addition, for both pitch-axis locations, increasing Ω_0^+ enhances this apparent camber effect. According to the experiments of Lambourne and Bryer,[27] positive camber promotes a delay in vortex breakdown for a fixed maximum local incidence. Another effect associated with the pitching motion is the variation of mean effective wing angle of attack $\bar{\alpha}_{\text{eff}}$, taken here for simplicity as the average of the minimum and maximum values of α_{eff}. With the pitch axis at the trailing edge, increasing Ω_0^+ further reduces $\bar{\alpha}_{\text{eff}}$, which tends to delay breakdown. However, for $X_0/C = 0.0$, increasing the pitch rate results in a higher effective wing incidence, which would promote vortex breakdown. Therefore, for the trailing-edge pivot location, the apparent camber and mean incidence effects both tend to delay bursting as the pitch rate is increased. However, for the apex pivot location, these two effects have opposite trends with increasing pitch rate.

The previous motion-induced effects on effective local angle of attack are in accordance with the more pronounced delay of vortex breakdown observed (Fig. 6b) with increasing Ω_0^+ when the pitch axis is at the trailing edge. They also correlate with the additional lag in vortex breakdown obtained (for fixed Ω_0^+) when the pitch axis is moved from the apex to the trailing edge (Fig. 6a).

In order to illustrate the effect of pitch rate and pitch axis placement on the transient flow development, the pressure along the vortex core is shown in Fig. 8 at $\alpha = 34$ deg. By comparison with Fig. 7b, it is clear that higher mean effective angle of attack results in higher maximum magnitude of suction and in a more severe overall adverse pressure gradient, which has been shown[28] to promote bursting. The effect of

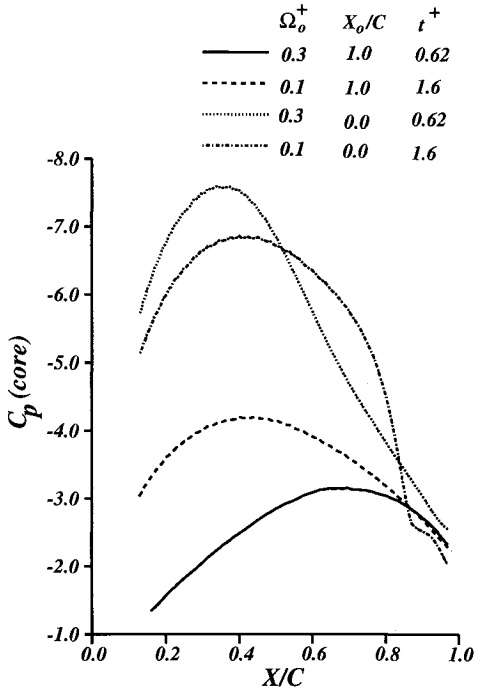

Fig. 8 Effect of Ω_0^+ and X_0/C on the pressure distribution along the vortex core at $\alpha = 34$ deg.

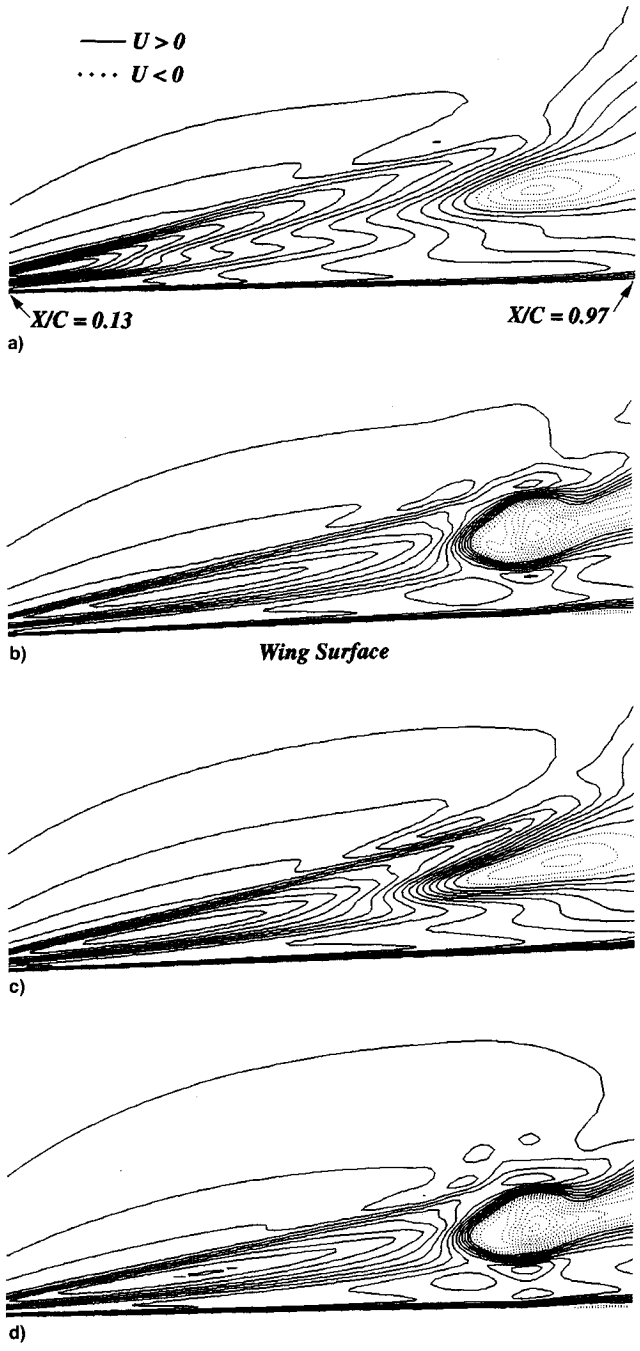

Fig. 9 Effect of Ω_0^+ and X_0/C on the flow structure (in terms of U contours) on longitudinal plane through vortex core when $X_b/C = 0.74$: a) $\Omega_0^+ = 0.3$ and $X_0/C = 1.0$, $\alpha = 50$ deg; b) $\Omega_0^+ = 0.1$ and $X_0/C = 1.0$, $\alpha = 43$ deg; c) $\Omega_0^+ = 0.3$ and $X_0/C = 0.0$, $\alpha = 39$ deg; and d) $\Omega_0^+ = 0.1$ and $X_0/C = 0.0$, $\alpha = 37$ deg.

motion-induced apparent camber is also clearly observed for the case of $\Omega_0^+ = 0.3$ and $X_0/C = 1.0$, which displays a favorable pressure gradient along the vortex core up to $X/C = 0.7$.

The effect of pitch rate and pitch-axis location on the swirl level in the vortex core was also examined at $\alpha = 34$ deg. An approximate measure of the swirl level was obtained by computing the swirl ratio $\Psi = |w|/u$ along lines in the spanwise direction passing through the center of the vortex. The maximum value of the swirl ratio Ψ at a given streamwise station (not shown) was found to increase, as expected, with effective angle of attack. For instance, for $\Omega_0^+ = 0.3$ and $X_0/C = 1.0$, the value of $\Psi_{\max} = 0.37$ is found, while for $\Omega_0^+ = 0.1$ and $X_0/C = 1.0$, $\Psi_{\max} = 0.65$. This decrease in swirl ratio

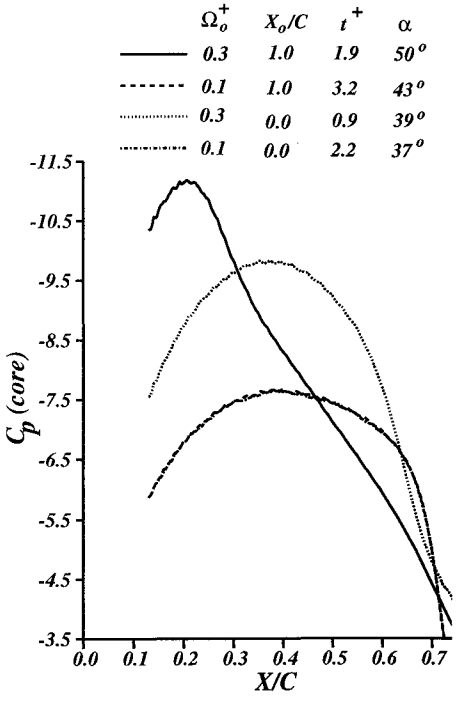

Fig. 10 Effect of Ω_0^+ and X_0/C on the pressure distribution along the vortex core when $X_b/C = 0.74$.

with increasing pitch rate is also consistent with the observed angular delay of breakdown.[29,30]

The flow structure was also examined at the instant when vortex breakdown has progressed in each case to $X_b/C = 0.74$. Figure 9 shows contours of the U component of velocity on a longitudinal plane normal to the wing and passing through the vortex center (see Fig. 1). In addition, the corresponding pressure along the vortex core is given in Fig. 10. For the high pitch rate (Figs. 9a and 9c), the reversed-flow region is less blunt and more axisymmetric as compared to the lower pitch rate cases (Figs. 9b and 9d) since less time has elapsed following the onset of breakdown. For the lower pitch rate cases, the formation of a bubble-type structure is already becoming apparent.

The flow structures in Figs. 9b and 9d are in remarkable agreement, and the core pressure distributions (Fig. 10) are essentially identical and appear as a single curve in the graph. This similarity is consistent with the equivalence in initial vortex breakdown propagation speeds previously noted for these cases in reference to Fig. 6a. The differences in time and angle of attack between Figs. 9b and 9d are approximately one convective time and 6.0 deg, respectively. This shift in angle of attack is very close to the difference in motion-induced effective incidence of 5.0 deg observed between these two cases in Fig. 7b. It is therefore seen that, for $\Omega_0^+ = 0.1$, the change in pitch-axis location simply amounts to a shift in time or α without significant modification of the flow structure. Based on this observation, experiments performed at the same pitch rate, but with different pivot location, can be correlated by a suitable shift in angle of attack. The higher pitch rate cases ($\Omega_0^+ = 0.3$) cannot be presently matched by a simple shift in time. For this to be possible, the maneuver with $\Omega_0^+ = 0.3$ and $X_0/C = 1.0$ would have to be continued beyond $\alpha = 50$ deg, given the large angular shift seen in Fig. 7b for the $\Omega_0^+ = 0.3$ cases.

Concluding Remarks

The effects of pitch rate and pitch-axis location on the onset and initial propagation of vortex breakdown above a pitching delta wing have been investigated numerically. Calculations were performed for a 75-deg sweep delta wing undergoing a ramp-type maneuver from $\alpha = 25$ to 50 deg. An assessment of numerical resolution adequacy, as well as comparison with experimental data were provided for validation purposes. For the range of the above parameters considered, the following conclusions were reached:

1) Increasing the pitch rate produced a further angular delay in the onset of breakdown, in agreement with previous experimental observations. This effect was more pronounced with the pitch-axis located at the trailing edge.

2) For a fixed pitch rate, moving the axis from the wing apex to the trailing edge resulted in an additional delay of breakdown characterized by a shift in angle of attack, but without significant alteration of the flow structure. This would permit the correlation of experimental data obtained with different axis locations.

3) At the relatively high pitch rates considered, trends 1 and 2 may be partially explained in terms of the effective local angle of attack along the wing induced by the imposed pitching motion.

References

[1]Skow, A. M., and Erickson, G. E., "Modern Fighter Aircraft Design for High-Angle-of-Attack Maneuvering," AGARD LS-121, Paper 4, 1982.

[2]Jarrah, M.-A., "Low-Speed Wind-Tunnel Investigation of Flow About Delta Wings, Oscillating in Pitch to Very High Angle of Attack," AIAA Paper 89-0295, Jan. 1989.

[3]Reynolds, G., and Abtahi, A., "Instabilities in Leading-Edge Vortex Development," AIAA Paper 87-2424, Aug. 1987.

[4]Bragg, M. B., and Soltani, M. R., "Measured Forces and Moments on a Delta Wing During Pitch-Up," *Journal of Aircraft*, Vol. 27, No. 3, 1990, pp. 262–267.

[5]Magness, C., Robinson, O., and Rockwell, D., "Control of Leading-Edge Vortices on a Delta Wing," AIAA Paper 89-0999, March 1989.

[6]Ekaterinaris, J. A., and Schiff, L. B., "Navier-Stokes Solutions for an Oscillating Double-Delta Wing," AIAA Paper 91-1624, June 1991.

[7]Visbal, M. R., "Onset of Vortex Breakdown Above a Pitching Delta Wing," *AIAA Journal*, Vol. 32, No. 8, 1994, pp. 1568–1575.

[8]Kandil, O. A., and Chuang, H. A., "Unsteady Delta-Wing Flow Computation Using an Implicit Factored Euler Scheme," AIAA Paper 88-3649, July 1988.

[9]Ashley, H., Katz, J., Jarrah, M.-A., and Vaneck, T., "Unsteady Aerodynamic Loading of Delta Wings for Low and High Angles of Attack," *International Symposium on Nonsteady Fluid Dynamics*, edited by J. Miller and D. Telionis, American Society of Mechanical Engineers Fluids Engineering Div., Vol. 92, 1990.

[10]Rockwell, D., "Three-Dimensional Flow Structure on Delta Wings at High Angle of Attack: Experimental Concepts and Issues," AIAA Paper 93-0550, Jan. 1993.

[11]Huyer, S., Robinson, M., and Luttges, M., "Unsteady Aerodynamic Loading Produced by a Sinusoidally Oscillating Delta Wing," AIAA Paper 90-1536, June 1990.

[12]Rediniotis, O., Klute, S., Hoang, N., and Telionis D., "Pitching-Up Motions of Delta Wings," AIAA Paper 92-0278, Jan. 1992.

[13]Magness, C., Robinson, O., and Rockwell, D., "Instantaneous Topology of the Unsteady Leading-Edge Vortex at High Angle of Attack," *AIAA Journal*, Vol. 31, No. 8, 1993, pp. 1384–1391.

[14]Pulliam, T. H., and Steger, J. L., "Implicit Finite-Difference Simulation of Three-Dimensional Compressible Flow," *AIAA Journal*, Vol. 18, No. 2, 1980, pp. 159–167.

[15]Beam, R. M., and Warming, R. F., "An Implicit Factored Scheme for the Compressible Navier-Stokes Equations," *AIAA Journal*, Vol. 16, No. 4, 1978, pp. 393–402.

[16]Pulliam, T., "Artificial Dissipation Models for the Euler Equations," *AIAA Journal*, Vol. 24, No. 12, 1986, pp. 1931–1940.

[17]Rai, M., and Chakravarthy, S., "An Implicit Form of the Osher Upwind Scheme," *AIAA Journal*, Vol. 24, No. 5, 1986, pp. 735–743.

[18]Gordnier, R. E., and Visbal, M. R., "Unsteady Vortex Structure over a Delta Wing," *Journal of Aircraft*, Vol. 31, No. 1, 1994, pp. 243–248.

[19]Webster, W. P., and Shang, J. S., "Comparison Between Thin-Layer and Full Navier-Stokes Simulations over a Supersonic Delta Wing," *AIAA Journal*, Vol. 29, No. 9, 1991, pp. 1363–1369.

[20]Gordnier, R., and Visbal, M., "Numerical Simulation of Delta-Wing Roll," AIAA Paper 93-0554, Jan. 1993.
[21]Visbal, M., "Structure of Laminar Juncture Flows," *AIAA Journal*, Vol. 29, No. 8, 1991, pp. 1273–1282.
[22]Stanek, M., and Visbal, M., "Investigation of Vortex Development on a Pitching Slender Body of Revolution," *Journal of Aircraft*, Vol. 30, No. 5, 1993, pp. 711–718.
[23]Visbal, M. R., "Computational Study of Vortex Breakdown on a Pitching Delta Wing," AIAA Paper 93-2974, July 1993.
[24]Lin, J.-C., and Rockwell, D., "Transient Structure of Vortex Breakdown on a Delta Wing," *AIAA Journal*, Vol. 33, No. 1, 1995, pp. 6–12.
[25]Visbal, M. R., and Gordnier, R. E., "Crossflow Topology of Vortical Flows," *AIAA Journal*, Vol. 32, No. 5, 1994, pp. 1085–1087.
[26]Ericsson, L. E., and Hanff, E., "Unique High-Alpha Roll Dynamics of a Sharp-Edged 65 Deg. Delta Wing," AIAA Paper 92-0276, Jan. 1992.
[27]Lambourne, N. C., and Bryer, D. W., "The Bursting of Leading-Edge Vortices—Some Observations and Discussion of the Phenomenon," Ames Research Center Reports and Memoranda 3282, April 1961.
[28]Sarpkaya, T., "Effect of Adverse Pressure Gradient on Vortex Breakdown," *AIAA Journal*, Vol. 12, No. 5, 1974, pp. 602–607.
[29]Sarpkaya, T., "On Stationary and Travelling Vortex Breakdowns," *Journal of Fluid Mechanics*, Vol. 45, Pt. 3, 1971, pp. 545–559.
[30]Faler, J., and Leibovich, S., "Disrupted States of Vortex Flow and Vortex Breakdown," *Physics of Fluids*, Vol. 20, No. 9, 1977, pp. 1385–1400.